# Electrically Tunable Quasi-3-D Mushroom Plasmonic Crystal

Qiugu Wang, Weikun Han, Peng Liu, and Liang Dong

***Abstract*—This paper reports an electrically tunable plasmonic crystal incorporating a nematic liquid crystal (LC) layer on the top surface of quasi-3-D mushroom plasmonic nanostructures. The presented plasmonic crystal is formed by an array of polymeric mushroom nanoposts with gold disks at the top and perforated nanoholes in a gold thin film at the bottom. The coupling between surface plasmon polariton (SPP) and Rayleigh anomaly (RA) is observed in experiments with quasi-3-D plasmonic crystals, and verified by simulations. The coupled SPP-RA resonance mode has its electric field vector prominently normal to the surface of the plasmonic nanostructures, and extends into the surrounding medium. This feature makes the coupled resonance sensitive to molecular reorientation in LC, and thus, is useful for designing index modulation-based tunable plasmonic crystal devices. Therefore, by applying external voltages across the LC layer, the SPP-RA resonance mode shows a redshift of 8 nm with a 35% change in the amplitude.**

***Index Terms*—Liquid crystal, microelectromechanical devices, optical surface waves.**

## I. Introduction

NANOPLASMONICS provides an efficient way to control and manipulate light in the vicinity of a metal surface below the diffraction limit through the excitation of surface plasmons (SPs) [1]. The Rayleigh anomaly (RA) is a non-resonant diffraction effect caused by light diffracting into an extended propagating in-plane wave [2]–[4]. This differs from surface plasmon polariton (SPP) resonance, which decays much more quickly away from the metal surface [4]–[6]. As has been previously studied, the coupling of RA and SPP [5], [6], and the coupling between RA and localized surface plasmon resonance (LSPR) [7]–[12] in planar plasmonic nanostructures, can lead to a stronger and narrower hybridized resonance. Quasi-3D plasmonic crystals are structured by an array of metal nanodisk-nanohole pairs physically separated by dielectric nanoposts or air-filled nanowells [13]–[20]. Because of the nanoscale distance between the nanodisks and nanoholes, a variety of hybridized SP modes exist with higher electric-field enhancement than the sole SPPs found in conventional planar nanohole-based plasmonic structures [13]–[18]. Quasi-3D plasmonic crystals can support RA, SPP and LSPR and can be fabricated in large-area arrays using soft nanoimprinting lithography, giving unique plasmonic performance [13]–[20]. For example, the coupled LSPR-RA resonance resulted in a high figure of merit value approaching the theoretical limit for standard propagating SP sensors [12].

Quasi-3D plasmonic nanostructures have demonstrated their capabilities in SP resonance-based sensing [13]–[16], imaging [13], and surface enhanced Raman spectroscopy [19], [20] in the visible and near-infrared wavelengths. However, if their optical responses are dynamically tunable, the quasi-3D nanostructures will become more useful when adapting to different applications. Therefore, we are interested in realizing an unexplored capability to actively control plasmonic fields in quasi-3D plasmonic crystals. A simple way to tune their optical response is to modulate their refractive index environment by using an active medium. Among many possible active media, liquid crystal (LC) has been extensively used to tune properties of many optical structures and devices [21]–[31] due to its large and controllable optical anisotropy and its versatile driving methods, including electrical [21]–[25], optical [26], [27], thermal [28], [29], and acoustic tuning [30].

In this paper, we demonstrate an electrically tunable quasi-3D plasmonic crystal using a thin layer of nematic LCs (Fig. 1(a)). This plasmonic nanostructure is formed by a periodic array of mushroom nanoposts with Au disks and nanoholes perforated in an Au thin film at the bottom (Fig. 1(b)-(e)). A shallow LC cell is created between the Au thin layer and a transparent conducting glass. We show that the introduction of the LCs allows for a redshift of an SPP mode excited at the Au disks to couple to the RA at the perforated Au film. The characteristic SPP-RA resonance field is predominately normal to the nanostructured surface and penetrates into the surrounding LC, thus making the resonance sensitive to reorientation of LC molecules. By applying an electric field applied across the LC cell of 0.55 V/$\mu$m, an 8 nm resonance shift with a 35% change in amplitude for the SPP-RA mode is observed.

## II. Device Fabrication

To fabricate the proposed tunable quasi-3D plasmonic crystal, we first utilize soft lithography-based replica molding process to form a polymer nanopost array made of polydimethylsiloxane (PDMS) elastomer. In this step, a silicon template is used as a solid master mold containing a square array of nanoposts. The master mold is silanized with (tridecafluoro-1, 1, 2, 2-tetrahydrooctyl)-1-trichlorosilane (T2492-KG, United Chemical Technologies) in a desiccator under active vacuum for 20 min. Then, an h-PDMS precursor solution is prepared by mixing poly (7–8% vinylmethyl-siloxane)- (dimethylsiloxane) (Gelest # VDT-731), (1, 3, 5, 7-tetravinyl-1, 3, 5,

Manuscript received August 25, 2015; revised January 15, 2016; accepted January 28, 2016. Date of publication February 7, 2016; date of current version March 18, 2016. This work was supported by the National Science Foundation under Grant ECCS # 0954765. The work of P. Liu was supported by the China Scholarship Council.

The authors are with the Department of Electrical and Computer Engineering, Iowa State University, Ames, IA 50011 USA (e-mail: qgwang@iastate.edu; kunhan@iastate.edu; pengliu@iastate.edu; ldong@iastate.edu).

Color versions of one or more of the figures in this paper are available online at http://ieeexplore.ieee.org.

Digital Object Identifier 10.1109/JLT.2016.2526634

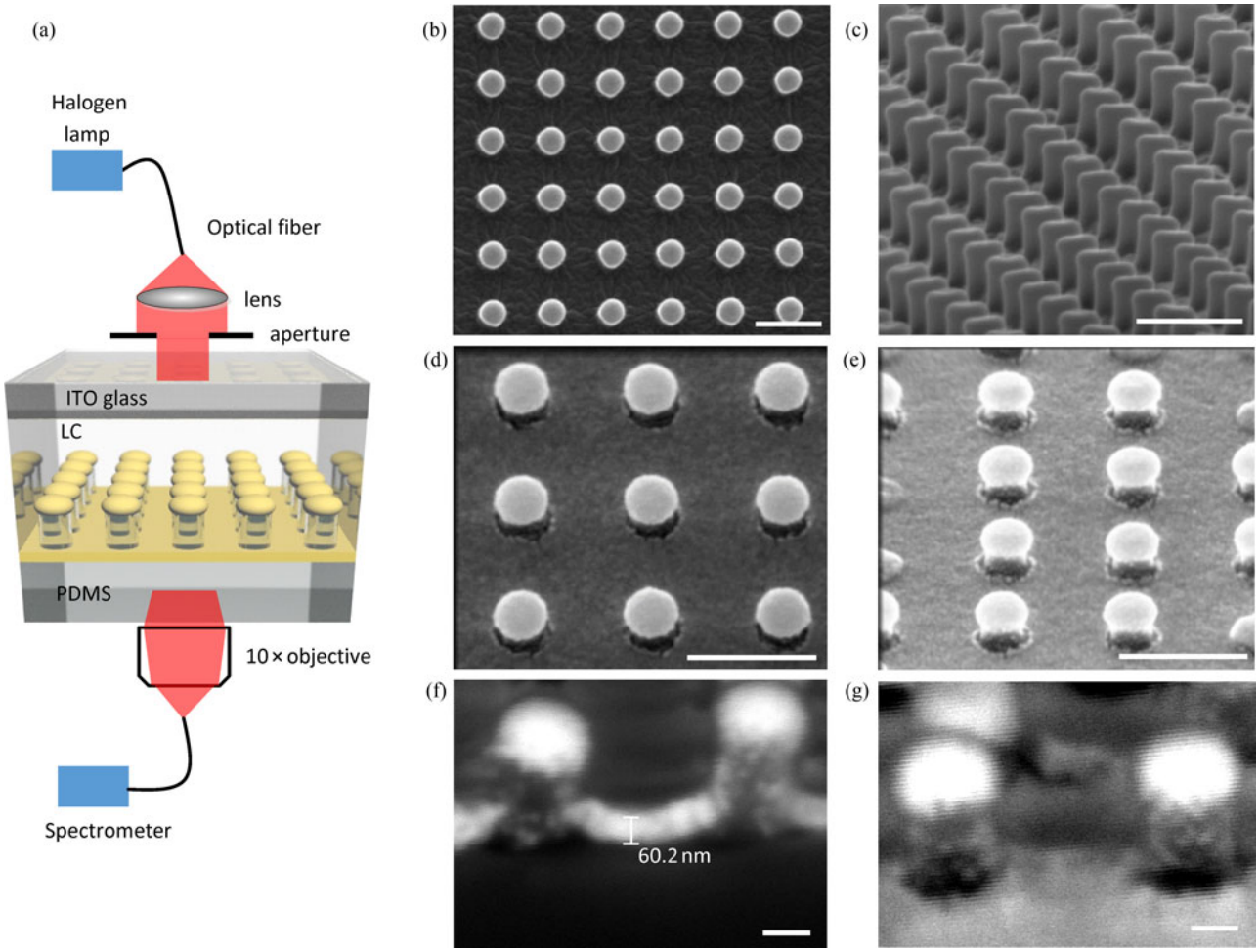


Fig. 1. (a) Schematic of an electrically tunable quasi-3D plasmonic crystal in a transmission measurement setup. (b), (c) Top and 45° side-view scanning electron microscopy (SEM) images for an array of polymer nanoposts without Au nanodisks (lattice constant $a = 500$ nm, post diameter $= 190$ nm, post height $= 300$ nm). (d), (e) 10° and 30° tilt view of the nanopost array deposited with a Ti/Au thin film. Scale bars in (b)-(e) represent 500 nm. (f), (g) Cross section and close-up of the nanoposts deposited with a Ti/Au thin film. Scale bars in (f) and (g) represent 100 nm.

7-tetramethylcyclotetrasiloxane) (Gelest # SIT7900.0), platinum catalyst Xylene (Gelest # SIP6831.2) and poly (25–30% methylhydro-siloxane)-(dimethylsiloxane) (Gelest # HMS-301) at the weight ratio of 3.4: 0.1: 0.05: 1. Air bubbles are removed from the mixture in a degassing chamber for 10 min, followed by spin-coating of the mixture onto the silicon mold at 1000 rpm for 40 sec and curing at 70 °C for 10 min. Subsequently, an s-PDMS precursor solution is prepared by mixing Sylgard 184 (Dow Corning, USA) and curing agent at the weight ratio of 10: 1 and degassing in a vacuum desiccator for 20 min. The s-PDMS mixture is then poured onto the top surface of the h-PDMS and cured on a hotplate at 65 °C for 2 hr. After that, the PDMS slab containing a square array of nanoholes is peeled from the silicon mold.

To form an array of polymer nanoposts shown in Fig. 1(c), the PDMS nanoholes obtained in the last step are used as a soft mold. This soft mold is treated with saline, coated with h-PDMS, and poured over with s-PDMS using the exactly same procedures as those used to make the soft mold. After that, the PDMS slab containing a square array of nanoposts is peeled from the soft mold. The obtained nanoposts have the period of 500 nm, the post diameter of 190 nm, and the post height of 300 nm. Finally, a 5 nm thick titanium (Ti) adhesion layer and a 60 nm thick Au layer are deposited on the whole surface of the device by using e-beam evaporation.

To obtain a uniform and large-area homeotropic alignment of nematic LCs (6CHBT; 1-(trans-4-Hexylcyclohexyl)-4- isothiocyanatobenzene, Sigma-Aldrich, USA) at the Au surface of the nanostructure, we functionalize the Au surface with a fluorinated silane-coupling agent (SCA, trichloro(1H, 1H, 2H, 2H-heptadecafluorodecyl) silane, Tokyo Chemical Industry, Japan) using a vapor-phase deposition method [32]. In this process, the PDMS-based array of nanoposts, an indium tin oxide (ITO) conducting glass, and a drop of silane-coupling agent (SCA, trichloro-1H, 1H, 2H, 2H-heptadecafluorodecyl silane, Tokyo Chemical Industry, Japan) are placed inside an active vacuum desiccator at room temperature for 5 min, and then is left for another 25 min to complete the deposition process. The formation of a monolayer SCA on nanostructure surface makes it strongly hydrophobic, allowing for homeotropic anchoring

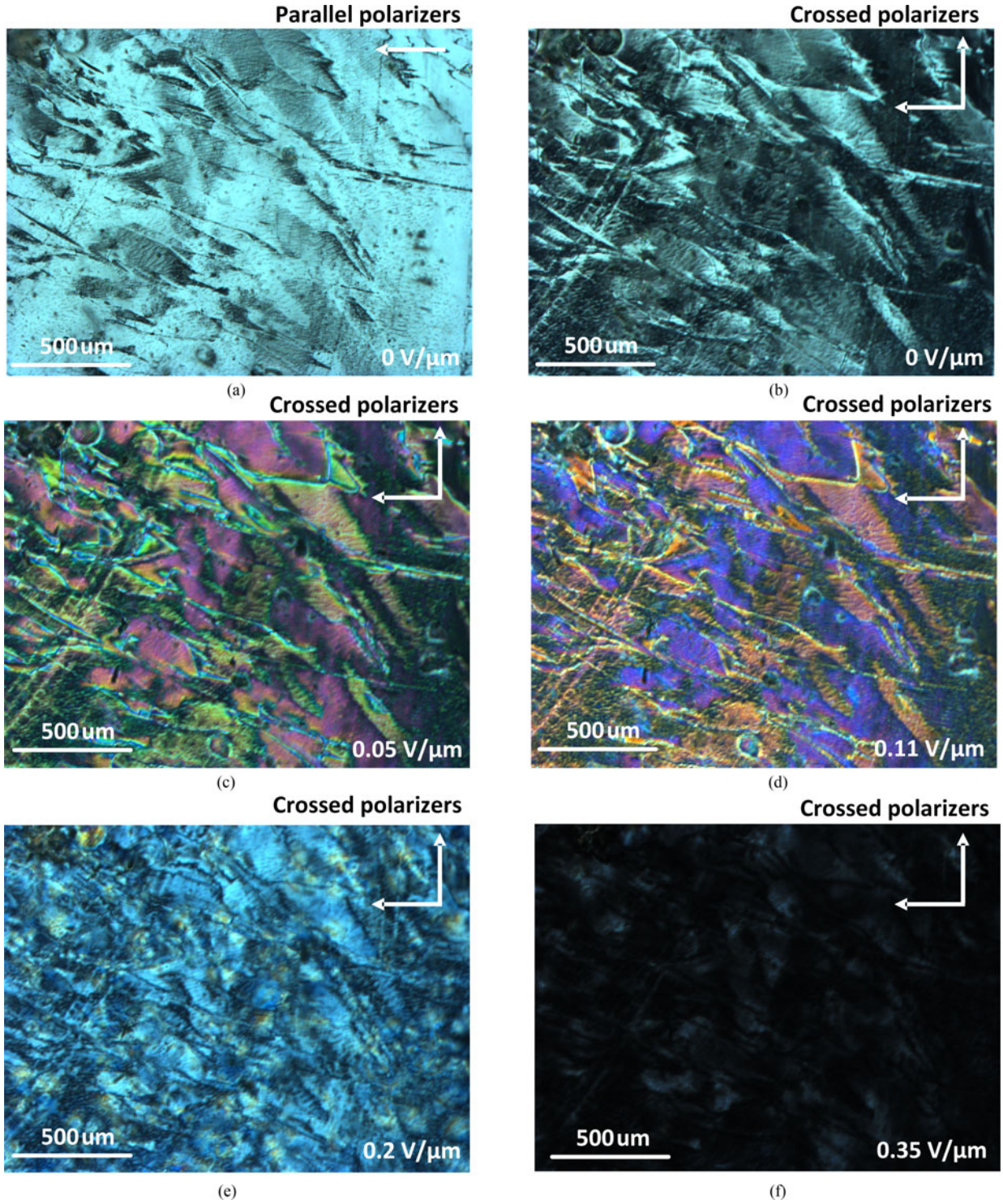


Fig. 2. Microscopic transmission images of the device under different electric fields. The upper and lower electrode surfaces of the 100 $\mu$m-deep LC cell are treated with SCA. (a) No electric field with two parallel polarizers; (b) No electric field with crossed polarizers; (c)-(f) Different electric fields with crossed polarizers. The field strength in each case is given in each panel.

and aligning of LC molecules at the nanostructure surface. The LC cell is then formed by placing a conducting ITO glass 100 $\mu$m away from the Au surface by using a double-sided silicone adhesive tape (Caplinq, UK). Lastly, the LCs are infused into the cell through a hole preformed in the ITO glass.

To verify the efficacy of the SCA treatment, two polarizers (Thorlabs, USA) are first arranged with their polarization directions parallel to each other and no electric field is applied to the device. In this case, the microscopic transmission image of LC textures appears quite bright (Fig. 2(a)). Subsequently,

the polarizers are oriented orthogonally with each other and microscopic transmission images of LC textures under different electric fields are taken (Fig. 2(b)-(f)). As shown in Fig. 2(b), before applying an electric field, the microphotograph of LCs under the crossed polarizers do not become totally dark, indicating that the LC molecules are partially isotropic. This is because the upper and lower electrodes of the cell is 100 $\mu$m apart, the interaction between the LC molecules and SCA-treated surfaces may not be sufficient enough to homeotropically align all the LC molecules. However, after an electric field is applied with increasing field strength, the microphotographs of LCs with the crossed polarizers gradually become darker (Fig. 2(c)-(e)). At the field strength of 0.35 V/$\mu$m, the LC cell turns to almost completely dark (Fig. 2(f)), indicating that under this electric field condition, all the LC molecules in the cell become almost homeotropically aligned to both the upper and lower electrode surfaces treated with SCA.

## III. Results and Discussion

It should be noted that the optical properties of quasi-3D plasmonic crystals are generally attributed to many possible resonance modes, including SPP at the Au/media interface, LSPR at the Au nanodisks and nanoholes, and non-resonant RA. The coupling effect of these modes will lead to further rich optical phenomena. Specifically, excitation wavelengths of the SPP and RA change with angle of incidence or surrounding index. Mode coupling between the SPP and RA may further be obtained through index modulations, which recently was demonstrated in planar plasmonic nanohole arrays [5], [6]. In addition, coupled SP resonances may also exist at the Au nanodisks and nanoholes due to their nanoscale distance, which leads to Fabry–Pérot (FP) resonance, as previously reported [12], [16, [18]. The resulting RA-FP resonance mode has a small full width at half maximum, a useful feature that enables high index sensitivity approaching the theoretical limit [12]. In the tunable quasi-3D plasmonic nanostructure presented here, electrical modulation of the effective index of LC will change the coupled resonance between the SPP at the medium/Au interface and the RA excited by the grating effect in the PDMS substrate, which will be discussed later.

To identify the underlying physics of the transmission features of the device, we first measure zero-order transmission spectra with normal incident light to the device surface exposed to air ($n = 1.00$) and different index liquids, including methanol ($n = 1.33$), ethanol ($n = 1.36$), isopropyl alcohol (IPA) ($n = 1.38$), and LC ($n_{\text{eff}} = 1.59$) at room temperature [Fig. 2(a)]. The effective index of LC is calculated using $n_{\text{eff}}^2 = \frac{2}{3}n_o^2 + \frac{1}{3}n_e^2$ [28], where $n_{\text{o}} = 1.53$ and $n_e = 1.71$ [33], representing the ordinary and extraordinary indices, perpendicular to and along the molecule orientation, respectively, of the LCs. In the optical measurement setup (Fig. 1(a)), a collimated white light source is generated from a 150 watts quartz halogen lamp. The transmitted light through the device is collected by an optical fiber through a 10× magnification objective lens (NA = 0.25) and measured by a spectrometer. The measured transmission spectra are shown in the upper panel of Fig. 3(a). When the 3D-quasi plasmonic nanostructure is exposed to air, a transmission dip appears at 519 nm, and a broadband Fano-like resonance profile consisting of a minimum transmission is observed at 710 nm. Full wave numerical simulations are carried out by using a finite element analysis (FEA) method with the commercial COMSOL software, where the relative permittivity of Au is taken from experimental data [34]. In this simulation, periodic boundary conditions are applied at the boundaries in parallel with the light propagation direction. Two perfect match layers (PMLs) are placed above and below the nanostructure to absorb the scattered electromagnetic (EM) fields. Also, the substrate is considered to be infinitely thick by setting the refractive index of the PMLs to be the same as that of the substrate. As given in the lower panel of Fig. 3(a), the simulation results agree with the experimental results when the Au disk has a diameter of 190 nm and a thickness of 60 nm. Note that the close-up SEM image of nanoposts (Fig. 1(f) and (g)) shows that there exists subtle isolated nanoscale grains of Au on the sidewall of nanoposts. But, in our simulation, these Au grains are not included in the model, because previous reported simulation for a similar nanostructure (nanodisk-nanohole pairs separated by air-filled nanowells) has shown that the inclusion of these Au grains on the sidewall will only slightly suppress the resonance intensity and shift the resonant wavelength [13]. In Fig. 3(a), the formation of the dip $D_1$ at 519 nm is attributed to the overlap of (1, 0) SPPs at the air/Au nanodisk interface with the direct light transmission through the thin Au film at the bottom. The peak around the wavelength of 500 nm is due to the direct transmission of light through the Au film. As the real part of the gold dielectric constant becomes +1, it leads to transparency in the absence of damping [5], [13], [14]. For a square lattice, the free space incident wavelength to excite an SPP and the free space incident wavelength of the RA are given respectively by [2]:

$$\lambda_{\text{SPP}} = \frac{a}{\sqrt{i_1^2 + j_1^2}} \sqrt{\frac{\varepsilon_d \varepsilon_m}{\varepsilon_d + \varepsilon_m}} \tag{1}$$

$$\lambda_{\text{RA}} = \frac{a}{\sqrt{i_2^2 + j_2^2}} \sqrt{\varepsilon_d} \tag{2}$$

where $\varepsilon_d$ and $\varepsilon_m$ are the dielectric constant of the medium and Au, $a$ is the lattice constant, and $(i_1, j_1)$ and $(i_2, j_2)$ correspond to the order of SPPs and RA, respectively. According to (1), at a normal incidence in air, the calculated SPP resonance $\lambda_{\text{SPP}}$ (1, 0) at the air/Au interface is 539 nm, which is redshifted compared to the experimental and simulated resonant wavelength at 519 nm. Eq. 1 used to estimate the SPP resonant wavelength is generally considered accurate when the metal film is thick enough. In our experiment, since the thickness of Au is only 60 nm, the interaction of the resonance modes on two sides of the Au film is expected to lead to a blueshift of the measured and FEA simulated resonance, compared to the calculated resonant wavelength using eq. 1. As shown in the electric field distribution (Fig. 3(b)), the standing wave feature above the Au nanodisk and below the perforated Au film confirms the excitation of SPPs. At the peak $P_1$ of 710 nm, the strong interaction between the LSPRs at the Au nanodisk and the Au film leads to a broad FP resonance. This phenomenon

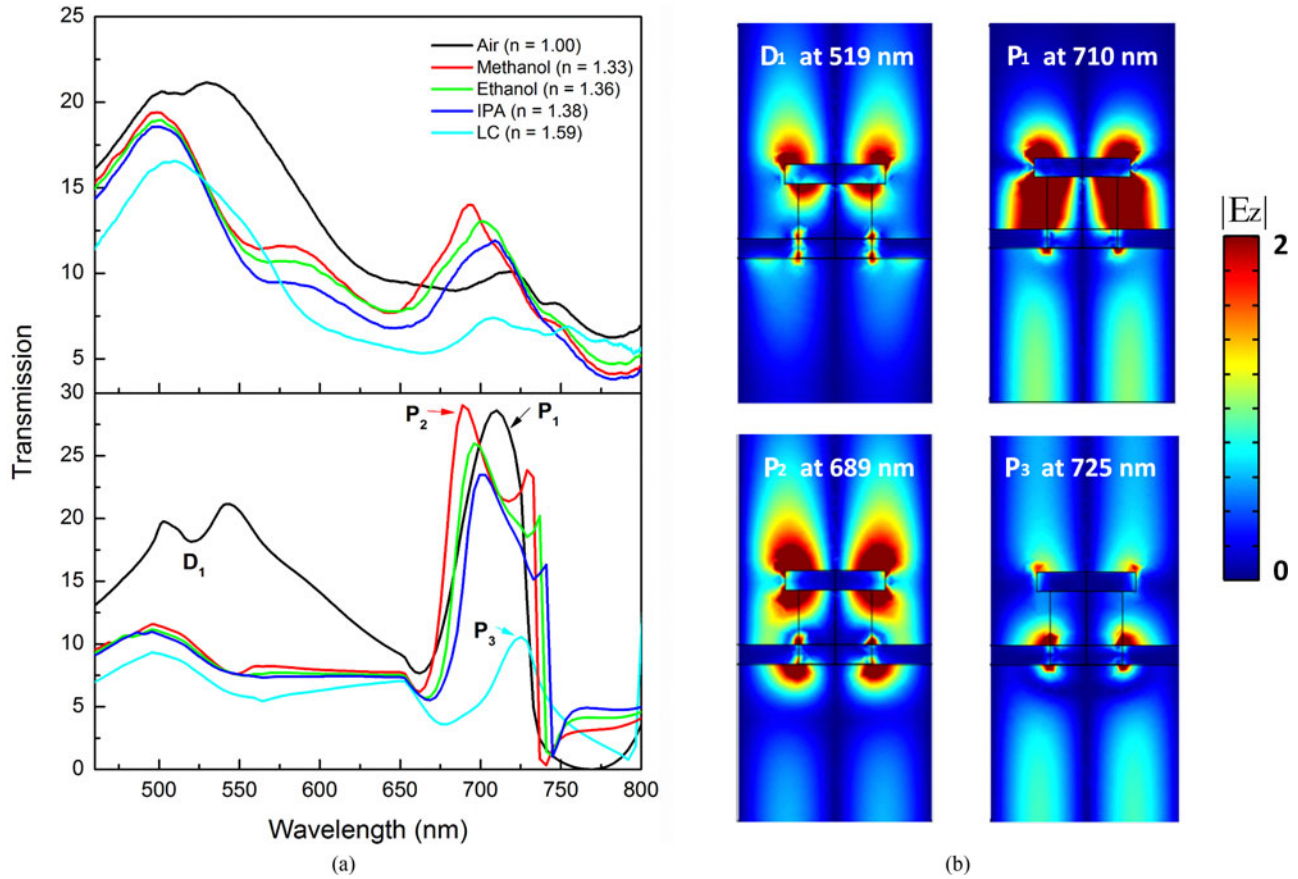


Fig. 3. (a) Plots in the upper panel show the measured transmission spectra of the quasi-3D plasmonic nanostructure under the normal incidence of light in different media. Plots in the lower panel show the corresponding simulated results. $D_1$, $P_1$, $P_2$, and $P_3$ in the simulated spectra indicate the transmission features of interest. $\lambda$D1 = 519 nm and $\lambda_{P1} = 710$ nm when the nanostructure surface was exposed in air; $\lambda_{P2} = 689$ nm when in methanol ($n = 1.33$); $\lambda_{P3} = 725$ nm when in LC ($n = 1.59$). (b) Simulated cross-sectional electric field distributions ($|Ez|$) at the resonant wavelengths mentioned above.

has also been observed in Ref. [12], [16], [18]. It is noteworthy that a weak standing wave feature appears in the resonance field distribution at $P_1$ in the PDMS substrate, but with a deeper field penetration into the substrate compared to the SPP resonance at $D_1$. This is attributed to the excitation of (1, 0) RA at the side of the PDMS substrate which is slightly blue-shifted with respect to the calculated RA wavelength at 730 nm, as estimated by (2). Although this RA mode has a relatively weak field intensity, the coupling between the SPP and RA at both sides of the thin Au film causes an enhanced transmission amplitude. As the surrounding medium changes to methanol ($n = 1.33$), a transmission peak with a larger amplitude emerges around 693 nm, which agrees with the simulation result for the peak $P_2$. The corresponding field distribution at $P_2$ (Fig. 3(b)) shows a similar pattern in the upper medium region to that at $D_1$, except for the region in the PDMS substrate where $(1, 0)_{\mathrm{PDMS}}$ RA occurs. According to (1), as the medium changes from air to methanol, the resulting (1, 0) SPP red-shifts to 705 nm and this leads to the coupling of $(1, 0)_{\mathrm{methanol/Au}}$ SPP and $(1, 0)_{\mathrm{PDMS}}$ RA. This SPP-RA coupling effect is similar to those that occurred in the planar plasmonic nanohole arrays where the coupling effect was achieved by tuning the position of RA [5], [6]. However, the SPP-RA resonance observed here is achieved by tuning the position of $\lambda_{\mathrm{SPP}}$ (1, 0) at the medium/Au nanodisk interface. Further increasing the index of the surrounding liquid medium to 1.36 and 1.38 causes the SPP-RA resonance to red-shift with a sensitivity of 517 refractive index units per nm (RIU/nm), while gradually decreasing its amplitude.

In the case that the index liquid medium uses LC ($n_{\mathrm{eff}} = 1.59$), both the experiment and simulation show the peak $P_3$ at 710 nm, but with a relatively lower amplitude compared to the peak $P_2$. The corresponding field distribution in Fig. 3(b) shows a similar pattern to $P_2$ but with a much deeper penetration depth, suggesting another coupled SPP-RA resonance. By using (1), $(1, 0)_{\mathrm{LC/Au}}$ SPP is predicted to be at 831 nm, while the (1, 1) order is at 651 nm. The relatively low amplitude at $P_3$, in comparison with the peaks caused by the coupling of (1, 0) SPP and RA, is due to two reasons: first, $(1, 1)_{\mathrm{LC/Au}}$ SPP is away from the strongest coupling position at 690 nm; second, $(1, 1)_{\mathrm{LC/Au}}$ SPP suffers more radiative losses than the (1, 0) order. However, the (1, 1) SPP electric field has a much deeper penetration rate into the medium than the (1, 0) order, which can be a benefit in designing LC-based plasmonic tunable devices.

With increasing applied electric field, the LC molecules tend to aligned with the electric field and become predominantly perpendicular to the substrate surface. Because the coupled

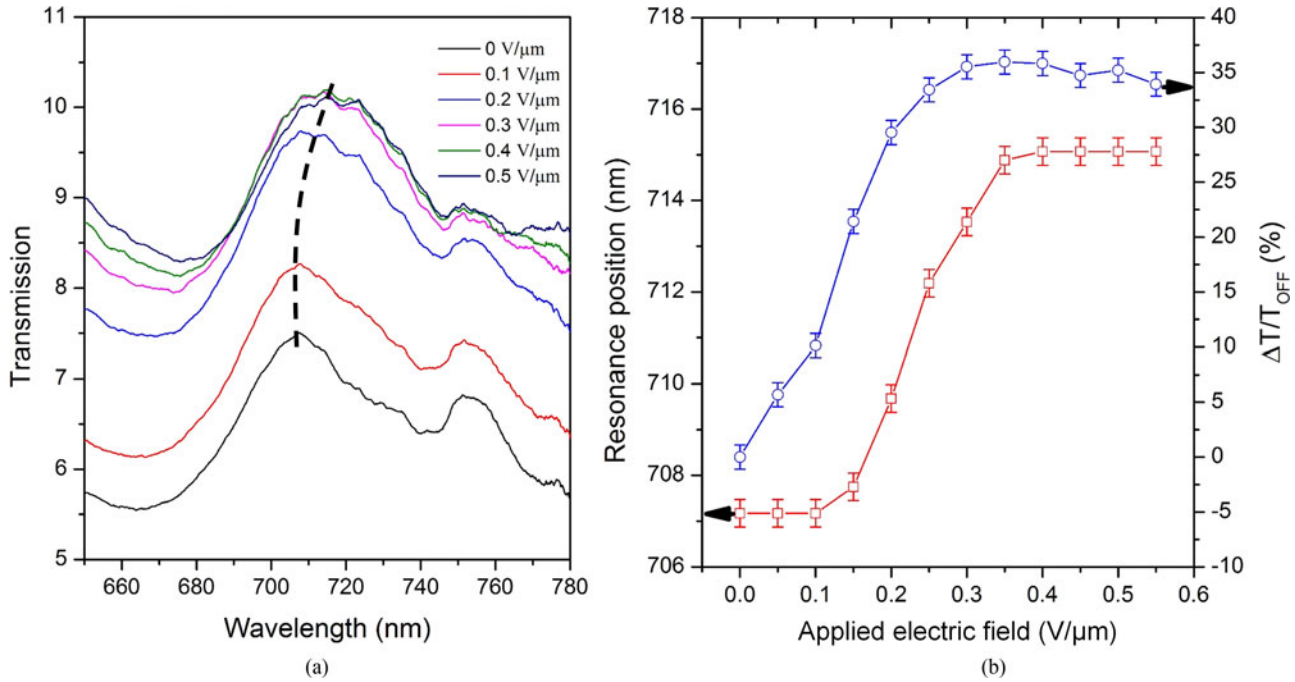


Fig. 4. (a) Transmission spectra of the LC-based quasi-3D plasmonic crystal at different applied electric field strengths. (b) Wavelength and relative transmission variation of the SPP-RA resonance as a function of applied electric field strength. $\Delta T = T_{ON} - T_{OFF}$, where $T_{ON}$ and $T_{OFF}$ represent transmission intensity when an external voltage is at the ON and OFF state, respectively.

SPP-RA mode has its electric field predominantly normal to the surface of the plasmonic nanostructure and extends up into the LC thin layer (as shown in Fig. 3(b)), the resonance characteristics of the device become sufficiently sensitive to index changes in the direction perpendicular to the LC/Au interface. Let us first assume the LC molecules experience a transition from a total isotropic state to a total homeotropic state. Under this assumption, the resulting maximum index variation in the perpendicular direction will be 0.12 or $n_e - n_{\text{eff}}$. Obviously, this theoretical index change is overestimated. Nevertheless, a redshift of the coupled SPP-RA resonance will still be expected. Fig. 4(a) shows the measured zero-order transmission spectra for different applied electric fields. By increasing the field strength to 0.55 V/$\mu$m, a maximum resonant wavelength shift of 8 nm with a 35% change in amplitude at the SPP-RA resonance is observed. Based on the measured resonance shift of 8 nm and the measured sensitivity of 517 RIU/nm mentioned above, the actual index change is calculated to be 0.015, which is much lower than the theoretical maximum value of 0.12 mentioned above. This is because the initial alignment of LC molecules is not fully homeotropic to the upper and lower electrode surfaces. After applying an electric field, the LCs tend to become homeotropic. Note that previous work on LC-based plasmonic switches also reported the resonance shift due to the LC reorientation from a partially homeotropic state to a homeotropic state [35].

In other reported LC-based tunable plasmonic devices using SPP or LSPR mode confined at the dielectric/metal interface, the SPP field usually has a longer decay length and can extend more into the surrounding medium, and thus exhibits higher sensitivity to the reorientation of LC molecules than the LSPR field does. Consequently, the LC devices using SPP mode require a lower operating electric field (e.g., ~1.25 V/$\mu$m [23]) than those using LSPR mode (e.g., ~2 V/$\mu$m [21] and 5 V/$\mu$m [22]). It should be pointed out that by coupling SPP and RA mode, our device has a higher field enhancement capability and allows extending the coupled field deeper into the LC layer. This unique feature leads to a lower operating electric field of ~0.55 V/$\mu$m of our device than the previously reported LSPR or SPP based LC devices [21]–[23].

## IV. Conclusion

In summary, we have demonstrated a LC-based electrically tunable quasi-3D plasmonic crystal, where both the experiment and simulation results have confirmed the coupling effect between RA and SPP resonance. The SPP-RA resonance field is predominantly normal to the surface of the plasmonic nanostructure and penetrates into the surrounding LC, which makes the resonance sensitive to the molecular reorientation of the LC. The ability of the device to tune its optical response suggests many potential applications in the areas of micro-display, sensing, and complex optical signal processing.

## Acknowledgment

The authors would thank Seval ÖREN for SEM imaging, Y. Wang for gold evaporation, and Dr. M. Lu and L. Liu for helpful discussions.

## REFERENCES


[1] W. L. Barnes, A. Dereux, and T. W. Ebbesen, "Surface plasmon subwavelength optics, " *Nature (Lond.)*, vol. 424, pp. 824–830, 2003.

[2] H. F. Ghaemi, T. Thio, and D. E. Grupp, "Surface plasmons enhance optical transmission through subwavelength holes, " *Phys. Rev. B*, vol. 58, pp. 6779–6782, 1998.

[3] M. Sarrazin, J. P. Vigneron, and J. M. Vigoureux, "Role of Wood anomalies in optical properties of thin metallic films with a bidimensional array of subwavelength holes, " *Phys. Rev. B*, vol. 67, p. 085415, 2003.

[4] J. M. Steele, C. E. Moran, A. Lee, C. M. Aguirre, and N. J. Halas, "Metallodielectric gratings with subwavelength slots: Optical properties, " *Phys. Rev. B*, vol. 68, p. 205103, 2003.

[5] J. M. McMahon, J. Henzie, T. W. Odom, G. C. Schatz, and S. K. Gray, "Tailoring the sensing capabilities of nanohole arrays in gold films with Rayleigh anomaly surface plasmon polaritons, " *Opt. Exp.*, vol. 15, pp. 18119–19129, 2007.

[6] H. Gao, J. M. McMahon, M. H. Lee, J. Henzie, S. K. Gray, G. C. Schatz, and T. W. Odom, "Rayleigh anomaly-surface plasmon polariton resonances in palladium and gold subwavelength hole arrays, " *Opt. Exp.*, vol. 17, pp. 2334–2340, 2009.

[7] E. M. Hicks, S. Zou, G. C. Schatz, K. G. Spears, and R. P. V. Duyne, "Controlling plasmon line shapes through diffractive coupling in linear arrays of cylindrical nanoparticles fabricated by electron beam lithography, " *Nano Lett.*, vol. 5, pp. 1065–1070, 2005.

[8] G. Vecchi, V. Giannini, and J. Gómez Rivas, "Surface modes in plasmonic crystals induced by diffractive coupling of nanoantennas, " *Phys. Rev. B*, vol. 80, p. 201401(R), 2009.

[9] V. G. Kravets, F. Schedin, and A. N. Grigorenko, "Extremely narrow plasmon resonances based on diffraction coupling of localized plasmons in arrays of metallic nanoparticles, " *Phys. Rev. Lett.*, vol. 101, p. 087403, 2008.

[10] W. Zhou and T. W. Odom, "Tunable subradiant lattice plasmons by out-of-plane dipolar interactions, " *Nat. Nanotechnol.*, vol. 6, pp. 423–427, 2011.

[11] M. Eitan, Z. Iluz, Y. Yifat, A. Boag, Y. Hanein, and J. Scheuer, "Degeneracy breaking of Wood's anomaly for enhanced refractive index sensing, " *ACS Photonics*, vol. 2, pp. 615–621, 2015.

[12] Y. Shen, J. Zhou, T. Liu, Y. Tao, R. Jiang, M. Liu, G Xiao, J. Zhu, Z. K. Zhou1, X. Wang, C. Jin, and J. Wang, "Plasmonic gold mushroom arrays with refractive index sensing figures of merit approaching the theoretical limit, " *Nat. Commun.*, vol. 4, p. 2381, 2013.

[13] M. E. Stewart, N. H. Mack, V. Malyarchuk, J. A. N. T. Soares, T. W. Lee, S. K. Gray, R. G. Nuzzo, and J. A. Rogers, "Quantitative multispectral biosensing and 1D imaging using quasi-3D plasmonic crystals, " *Proc. Nat. Acad. Sci. USA*, vol. 103, pp. 17143–17148, 2006.

[14] T. T. Truong, J. Maria, J. Yao, M. E. Stewart, T. W. Lee, S. K. Gray, R. G. Nuzzonand, and J. A. Rogers, "Nanopost plasmonic crystals, " *Nanotechnology*, vol. 20, p. 434011, 2009.

[15] F. J. Bezares, J. D. Caldwell, O. Glembocki, R. W. Rendel, M. Feygelson, M. Ukaegbu, R. Kasica, L. Shirey, N. D. Bassim, and C. Hosten, "The role of propagating and localized surface plasmons for SERS enhancement in periodic nanostructures, " *Plasmonics*, vol. 7, pp. 143–150, 2012.

[16] J. Xu, P. Kvasnička, M. Idso, R. W. Jordan, H. Gong, J. Homola, and Q. Yu, "Understanding the effects of dielectric medium, substrate, and depth on electric fields and SERS of quasi-3D plasmonic nanostructures, " *Opt. Exp.*, vol. 19, pp. 20493–20505, 2011.

[17] M. Najiminaini, F. Vasefi, B. Kaminska and J. J. L. Carson, "Transmission resonance of a three dimensional nano-structure with a localized surface plasmon property, " *Proc. SPIE*, vol. 8597, p. 859715, 2013.

[18] A. Artar, A. A. Yanik, and H. Altug, "Fabry–Pérot nanocavities in multilayered plasmonic crystals for enhanced biosensing, " *Appl. Phys. Lett.*, vol. 95, p. 051105, 2009.

[19] J. Xu, P. Guan, P. Kvasnicka, H. Gong, J. Homola, and Q. Yu, "Light transmission and surface-enhanced Raman scattering of quasi-3D plasmonic nanostructure arrays with deep and shallow Fabry-Perot nanocavities, " *J. Phys. Chem. C*, vol. 115, pp. 10996–11002, 2011.

[20] A. J. Baca, J. M. Montgomery, L. R. Cambrea, M. Moran, L. Johnson, J. Yacouband T. T. Truong, "Optimization of nanopost plasmonic crystals for surface enhanced Raman scattering, " *J. Phys. Chem. C*, vol. 115, pp. 7171–7178, 2011.

[21] P. A. Kossyrev, A. Yin, S. G. Cloutier, D. A. Cardimona, D. Huang, P. M. Alsing, and J. M. Xu, "Electric field tuning of plasmonic response of nanodot array in liquid crystal matrix, " *Nano Lett.*, vol. 5, pp. 1978–1981, 2005.

[22] K. C. Chu, C. Y. Chao, Y. F. Chen, Y. C. Wu, and C. C. Chen, "Electrically controlled surface plasmon resonance frequency of gold nanorods, " *Appl. Phys. Lett.*, vol. 89, p. 103107, 2006.

[23] W. Dickson, G. A. Wurtz, P. R. Evans, R. J. Pollard, and A. V. Zayats, "Electrically controlled surface plasmon dispersion and optical transmission through metallic hole arrays using liquid crystal, " *Nano Lett.*, vol. 8, pp. 281–286, 2008.

[24] Y. J. Liu, E. S. P. Leong, B. Wang, and J. H. Teng, "Optical transmission enhancement and tuning by overlaying liquid crystals on a gold film with patterned nanoholes, " *Plasmonics*, vol. 6, pp. 659–664, 2011.

[25] L. De Sio, A. Cuuningham, V. Verrina, C. M. Tone, R. Caputo, T. Bürgi, and C. Umeton, "Double active control of the plasmonic resonance of a gold nanoparticle array, " *Nanoscale*, vol. 4, pp. 7619–7623, 2012.

[26] V. K. S. Hsiao, Y. B. Zheng, B. K. Juluri, and T. J. Huang, "Light-driven plasmonic switches based on Au nanodisk arrays and photoresponsive liquid crystals, " *Adv. Mater.*, vol. 20, pp. 3528–3532, 2008.

[27] Y. Zhao, Q. Hao, Y. Ma, M. Lu, B. Zhang, M. Lapsley, I. Khoo, and T. J. Huang, "Light-driven tunable dual-band plasmonic absorber using liquid-crystal-coated asymmetric nanodisk array, " *Appl. Phys. Lett.*, vol. 100, p. 053119, 2012.

[28] S. Xiao, U. K. Chettiar, A. V. Kildishev, V. Drachev, I. C. Khoo, and V. M. Shalaev, "Tunable magnetic response of metamaterials, " *Appl. Phys. Lett.*, vol. 95, p. 033115, 2009.

[29] A. E. Cetin, A. Mertiri, M. Huang, S. Erramilli, and H. Altug, "Thermal tuning of surface plasmon polaritons using liquid crystals, " *Adv. Opt. Mater.*, vol. 1, pp. 915–920, 2013.

[30] Y. J. Liu, X. Ding, S. S. Lin, J. Shi, I. Chiang, and T. J. Huang, "Surface acoustic wave driven light shutters using polymer-dispersed liquid crystals, " *Adv. Mater.*, vol. 23, pp. 1656–1659, 2011.

[31] G. Si, Y. Zhao, E. S. P. Leong, and Y. J. Liu, "Liquid-crystal-enabled active plasmonics: A review, " *Materials*, vol. 7, pp. 1296–1317, 2014.

[32] H. Yoshida, T. Matsui, A. Miura, N. Ikeda, M. Ochiai, Y. Sugimoto, H. Fujikawa, and M. Ozaki, "Uniform liquid crystal alignment on metallic nanohole arrays by vapor-phase deposition of silane coupling agent, " *Opt. Mater. Exp.*, vol. 2, pp. 893–899, 2012.

[33] J. Baran, Z. Raszewski, R. Dabrowski, J. Kedzierski, and J. Rutkowska, "Some physical properties of mesogenic 4-(trans-4'-n-alkylcyclohexyl) isothiocyanatobenzenes, " *Mol. Cryst. Liq. Cryst.*, vol. 123, pp. 237–242, 1985.

[34] E. D. Palik, *Handbook of Optical Constants of Solids*, New York, NY, USA: Academic, 1985.

[35] Y. J. Liu, Q. Hao, J. S. T. Smalley, J. Liou, I. C. Khoo, and T. J. Huang, "A frequency-addressed plasmonic switch based on dual-frequency liquid crystals, " *Appl. Phys. Lett.*, vol. 97, p. 091101, 2010.


Authors' biographies not available at the time of publication.